Disruption of CCTβ2 Expression Leads to Gonadal Dysfunction

Suzanne Jackowski,[1,2]* Jerold E. Rehg,[3] Yong-Mei Zhang,[1] Jina Wang,[1] Karen Miller,[1]
Pam Jackson,[1] and Mohammad A. Karim[1]†

*Departments of Infectious Diseases[1] and Pathology,[3] St. Jude Children's Research Hospital, Memphis,
Tennessee 38105, and Department of Molecular Sciences, University of Tennessee
Health Science Center, Memphis, Tennessee 38163[2]*

There are two mammalian genes that encode isoforms of CTP:phosphocholine cytidylyltransferase (CCT), a key rate-controlling step in membrane phospholipid biogenesis. Quantitative determination of the CCT transcripts reveals that CCTα is ubiquitously expressed and is found at the highest levels in the testis and lung, with lower levels in the liver and ovary. CCTβ2 is a very minor isoform in most tissues but is significantly expressed in the brain, lung, and gonads. CCTβ3 is the third isoform recently discovered in mice and is expressed in the same tissues as CCTβ2, with its highest level in testes. We investigated the role(s) of CCTβ2 by generating knockout mice. The brains and lungs of mice lacking CCTβ2 expression did not exhibit any overt defects. On the other hand, a large percentage of the CCTβ2$^{-/-}$ females were sterile and their ovaries exhibited defective ovarian follicle development. The proportion of female CCTβ2$^{-/-}$ mice with defective ovaries increased as the animals aged. The rare litters born from CCTβ2$^{-/-}$ × CCTβ2$^{-/0}$ matings had the normal number of pups. The abnormal ovarian histopathology was characterized by disorganization of the tissue in young adult mice and absence of follicles and ova in older mice, along with interstitial stromal cell hyperplasia which culminated in the emergence of tubulostromal ovarian tumors by 16 months of age. Grossly defective CCTβ2$^{-/-}$ ovaries were associated with high follicle-stimulating (FSH) and luteinizing (LH) hormone levels. Male CCTβ2$^{-/0}$ mice exhibited progressive multifocal testicular degeneration and reduced fertility but had normal FSH and LH levels. Thus, the most notable phenotype of CCTβ2 knockout mice was gonad degeneration and reproductive deficiency. The results indicate that although CCTβ2 is expressed at very low levels compared to the α-isoform, loss of CCTβ2 expression causes a breakdown in the gonadal response to hormonal stimulation.

Phosphatidylcholine (PtdCho) is a major component of biological membranes in higher eukaryotes and is also secreted by specialized tissues for important extracellular tasks. CTP:phosphocholine cytidylyltransferase (CCT) is a key rate-controlling step in the major biosynthetic pathway leading to PtdCho in most tissues (for reviews, see references 15, 17, and 36). In mammals there are two genes, *Pcyt1a* (formerly *Cptct*), located on murine chromosome 16, and *Pcyt1b*, located on the X chromosome, that encode proteins termed CCTα and CCTβ, respectively (35, 38). The two genes exhibit tissue-specific expression, with CCTα predominating in most tissues and CCTβ being most abundant in brain tissue (32). Two transcripts arise from the *Pcyt1a* gene that encode the identical CCTα protein. Alternate splicing of the X-linked *Pcyt1b* gene directs the synthesis of two mRNAs that encode the CCTβ2 and CCTβ3 isoforms in mice (32, 35, 38). CCTβ3 is 28 residues shorter at the amino terminus than CCTβ2 due to transcript initiation at an alternate first exon (32). In humans, intron retention gives rise to a CCTβ1 transcript found in the expressed sequence tag database that is predicted to encode a smaller protein that lacks the carboxy-terminal domain (35).

However, the β1 isoform is not detected in mice (32), and there is no evidence that the CCTβ1 protein is expressed at significant levels in human tissues.

The CCT proteins are divided into four functional domains. The CCTα amino-terminal region contains a cluster of positively charged amino acids that specify nuclear localization (57–59), whereas the CCTβ proteins lack this signature sequence (32, 36). Thus, CCTα is predominantly a nuclear protein in most cell types (58), with the exception of lung cells (48), and a smaller amount of extranuclear CCTα is found associated with the endoplasmic reticulum (35). In contrast, CCTβ proteins are localized to the endoplasmic reticulum compartment and are absent from the nucleus (35). Both proteins have almost identical catalytic and regulatory helical domains, and accordingly the enzymatic activities of the α and β isoforms depend on their interaction with lipid regulators (35). The catalytic core (residues 72 to 233) is highly conserved among all cytidylyltransferases, from bacteria to mammals (47, 51). A phospholipid sensor domain, or helical domain (residues 256 to 288), is unique to the mammalian proteins and consists of three consecutive 11-residue repeats that form an amphipathic α-helix (30). The helical domain regulates the protein's reversible association with biological membranes (2, 18, 20, 30, 31) together with its activity (56, 64). The curvature elastic stress hypothesis (4) provides a theoretical framework for understanding both the positive and negative functions of specific membrane lipids in CCT regulation via the helical domain (4, 19). Both the α and β proteins have carboxy-

* Corresponding author. Mailing address: Protein Science Division, Department of Infectious Diseases, St. Jude Children's Research Hospital, 332 N. Lauderdale, Memphis, TN 38105-2794. Phone: (901) 495-3494. Fax: (901) 495-3099. E-mail: suzanne.jackowski@stjude.org.
† Present address: Division of Endocrinology, Department of Medicine, Central Arkansas Veterans Healthcare System and University of Arkansas for Medical Sciences, Little Rock, AR 72205.

terminal domains with multiple phosphorylation sites (35). Increased phosphorylation attenuates the activation of CCTα by lipid mediators (3, 65), phosphorylated CCTα is often found dissociated from the cell membrane (55), and the carboxy-terminal domain itself also imparts regulation of enzymatic activity by anionic lipids (37). The function of the CCTβ2 carboxy terminus in controlling activity has not been investigated, but the amino acid sequences of the carboxy-terminal domains of the mouse α, β2, and β3 isoforms are 49% identical (57% similar), suggesting that the proteins are regulated similarly by anionic lipids and phosphorylation. Truncation of both the helical and carboxy-terminal domains gives rise to a dysregulated CCTα that has higher basal activity in the absence of lipid and is refractory to lipid stimulation (for a review, see reference 36).

The biochemical data thus far has not distinguished a unique, nonredundant role for the CCTβ isoforms in cell or tissue function. A few clues about the regulation of CCTα have emerged from studies with cell culture models, but CCTβ proteins were not detected in these systems. Redistribution of CCTα from a predominantly nuclear location to extranuclear sites is associated with growth factor stimulation of PtdCho synthesis (45). Transient elevation of CCT activity in response to apoptosis is accompanied by increased CCTα availability in the extranuclear compartment (34). While these two studies suggest that CCTα outside the nucleus supports a quantitative increase in or replacement of bulk cellular PtdCho, CCTα within the nucleus is also thought to be functional, because the nuclear phospholipids contains unique PtdCho molecular species (28). Overexpression of CCTβ2 or CCTβ3 protein complements a mutant cell line with conditionally defective endogenous CCT activity (32), as does overexpression of CCTα or even catalytically compromised CCTα mutant proteins (37). Acceleration of PtdCho synthesis by the overexpression of CCT is counteracted by the ability of cells to degrade PtdCho to glycerophosphocholine and to maintain a constant cellular phospholipid content (5, 53). These studies reveal the existence of a homeostatic mechanism(s) for biochemical control over membrane phospholipid biosynthesis (5, 7, 14), but they shed no light on the role of the specific CCT isoforms or their regulatory domains in cell physiology.

To overcome the difficulties of using cell lines and overexpression studies, we developed a sensitive, quantitative method to determine the relative levels of the CCT transcripts expressed in mouse tissues. We compared these values to those for the phosphatidylethanolamine methyltransferase (PEMT), which governs the alternate pathway for PtdCho synthesis in liver (52), to obtain a sense of the relative contributions of each of these proteins to PtdCho synthesis overall. We found that CCTβ2 and CCTβ3, if expressed, constitute a minor species in most tissue CCT pools, except for brain tissue. To investigate whether CCTβ2 has a unique role in a select tissue(s), we derived a mouse strain which lacks expression of the CCTβ2 isoform. We found that these animals have marked gonadal defects pointing to an important role for CCTβ2 in reproductive physiology.

MATERIALS AND METHODS

Isolation of murine CCTβ genomic clones. A mouse genomic 129/SvE library in λEMBL3 (gift from Gerard Grosveld, Department of Genetics, St. Jude

Children's Research Hospital) was screened with the d[α-^{32}P]CTP-labeled human 0.9-kb (BamHI-EcoRI) fragment of the CCTβ2 cDNA from plasmid pAL2 (35). Plaque hybridization was performed for 14 h at 42°C in a solution of 25% formamide, 0.75 M NaCl, 75 mM sodium citrate, 2× Denhart's solution (0.02% bovine serum albumin, 0.02% Ficoll, 0.02% polyvinylpyrorolidone), 20 mM sodium phosphate buffer (pH 6.5), 0.1% sodium dodecyl sulfate (SDS), 100 μg of salmon sperm DNA/ml, 10% dextran sulfate. The nitrocellulose filters (Schleicher & Schuell, Dassel, Germany) were washed at 55°C for 1 h in a solution of 0.1× SSC (1× SSC is 0.15 M NaCl plus 0.015 M sodium citrate) and 0.1× SDS and were exposed to film. After secondary and tertiary screening, a positive plaque was isolated by using the QIAGEN Lambda kit, the DNA was digested with BamHI, and a 9.0-kb fragment was subcloned into the vector pBluescript KS(+). The sequence of the mouse CCTβ2 fragment was determined and found to contain the entire exon 2 in the murine *Pcyt1b* gene structure (32) plus 857 bp of upstream and 5,948 bp of downstream intronic sequences.

Construction of the CCTβ2 replacement vector. In general, the *Neo* resistance gene cassette was inserted into exon 2 of the CCTβ gene and a portion of the 3′ coding sequence from exon 2 was deleted. A negative selection cassette encoding the diphtheria toxin antigen (DTA) was added at the 3′ end of the mouse genomic DNA insert. To accomplish this addition, synthetic oligonucleotides were used to construct a new multiple cloning site that was inserted in pBluescript KS(+) to yield pMAK6. Next the 1,459-bp HindIII-NcoI fragment of CCTβ2 exon 2 DNA was subcloned into pMAK6, followed by the 6-kb PstI-BamHI gene fragment. This removed 35 bp of coding sequence from exon 2 and 122 bp of the downstream intron. The 1.2-kb DTA selection cassette (a gift from James Ihle, Department of Biochemistry, St. Jude Children's Research Hospital) was inserted by using XhoI and ClaI. Finally, the 1.2-kb XbaI-EcoRV *Neo* resistance gene cassette was inserted. The DNA sequence of the plasmid was verified, and the insert is depicted in Fig. 1A.

Generation and identification of gene-targeted ES cell clones. KpnI was used to linearize the replacement vector prior to transfection into the 129/Sv-+p+Tyr-cMgfSl-J/+ substrain of embryonic stem cells, W9.5 (gift from Peter McKinnon, Department of Genetics, St. Jude Children's Research Hospital), grown on mitotically inactivated mouse embryonic fibroblasts which carry resistance to neomycin. More than 200 clones resistant to G418 were selected and screened by Southern blot analysis by using a 207-bp PstI-HindIII probe corresponding to the 5′ end of exon 2 outside the targeted portion (Fig. 1A). Genomic DNA (10 μg) from individual embryonic stem (ES) cell clones was digested with BamHI and separated on a 0.8% agarose gel. After transfer to Nylon membrane (Hybond-N$^+$; Amersham Pharmacia Biotech), hybridization was performed by using Quickhyb solution (Stratagene) containing 1×10^6 to 2×10^6 cpm of ^{32}P-labeled probe/ml at 42°C overnight. After being washed the blot was exposed to a phosphor screen for 1 to 4 days and was scanned. ES cells that had undergone homologous recombination on the X chromosome with the replacement vector were identified by a 2.8-kb band instead of the 9.0-kb wild-type band (Fig. 1B).

Cell culture. Rat pheochromocytoma (PC12) cells were obtained from the American Type Culture Collection (ATCC) and were maintained in Ham's F12 medium (ATCC) with 15% horse serum (Atlanta Biologicals, Inc.), 2.5% fetal bovine serum (Atlanta Biologicals, Inc.), 10 mM HEPES (Invitrogen), 2 mM glutamine (Invitrogen), and 5% CO_2 at 37°C. For experiments with nerve growth factor (NGF; Invitrogen), cells were harvested without trypsinization and were plated on 100-mm-diameter collagen-coated petri dishes (Becton Dickinson) at a density of 20%, followed by incubation for 24 h. NGF (100 ng/ml) was then added to the indicated cultures and also when the medium was changed 3 days later. After 5 days of incubation with NGF, both the untreated control dishes and the NGF-treated cultures were confluent and cells were washed with phosphate-buffered saline (PBS), lysed with TRIZOL reagent (Invitrogen) for RNA isolation, scraped into PBS without calcium or magnesium (Invitrogen) for protein determination (10) by using rabbit immunoglobulin as a standard, or trypsinized for cell counting by using a hemocytometer.

Generation and identification of CCTβ2-disrupted mice. Cells from a 129/Sv-+p+Tyr-c MgfSl-J/+ (W9.5) ES cell colony containing the recombined *Pcyt1b* DNA at the correct locus were injected into C57BL/6J blastocysts, which were then implanted into pseudopregnant female mice by the St. Jude Transgenic Core Facility. Male offspring with 75 to 90% agouti color, the coat color contributed by the ES cells, were bred with C57BL/6J females. Pups that were 100% agouti, indicating germ line transmission, were screened. Tail clips from weanling animals were digested overnight at 55°C in buffer containing 0.25 mg of proteinase K/ml, 0.2 M NaCl, 100 mM Tris-HCl (pH 8.5), 5 mM EDTA, and 0.2% SDS. The DNA was extracted by using an equal volume of phenol-chloroform:isoamyl alcohol, and the upper phase was precipitated with 0.8 volumes of cold isopropanol. The DNA precipitate was washed with 80% ethanol and was dissolved in 50 to 100 μl of water at 50°C for 30 min. The DNA was then subjected to
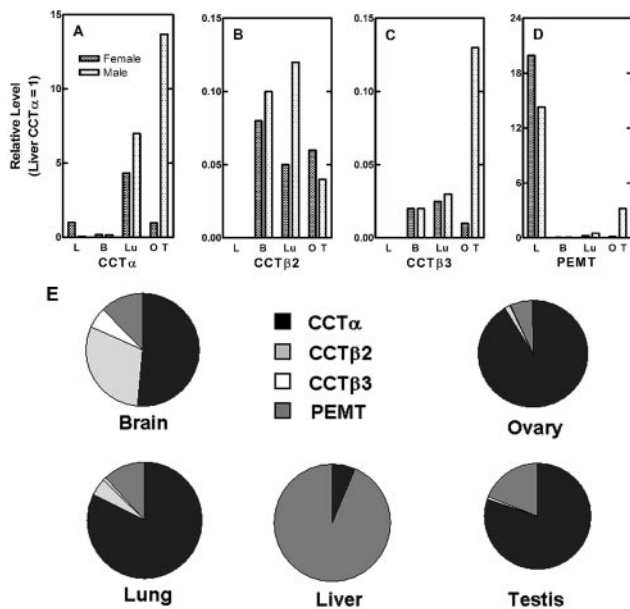
FIG. 1. Quantitation of the CCT and PEMT transcripts in mouse organs. (A to D) Selected organs were removed from male (hatched bars) and female (stippled bars) wild-type animals, RNA was isolated, and real-time PCR with 0.5 μg of template RNA and the ABI Prism 7700 Sequence Detection System was performed by using primers and probes specific for CCTα (A), CCTβ2 (B), CCTβ3 (C), PEMT (D), and GAPDH transcripts. Liver (L), brain (B), lung (Lu), ovary (O), and testis (T) from at least three mice of each gender were evaluated in quintuplicate and, by using the comparative C_T method, the amount of target RNA ($2^{-\Delta\Delta C_T}$) was normalized to the endogenous GAPDH reference (ΔC_T) and was related to the amount of target CCTα in liver ($\Delta\Delta C_T$), which was set as the calibrator at 1.0. Standard deviations from the mean ΔC_T values (not shown) were <10%. Tissues from both female (stippled bars) and male (cross-hatched bars) mice were analyzed. (E) Distribution of CCT and PEMT transcripts was calculated for individual organs by using data obtained from real-time PCR quantification (shown in panels A to D).

Southern analysis by using the exon 2 outside probe as described above. Heterozygous (+/−) females and homozygous (−/0) males were identified and sibmated to yield homozygous (−/−) females as identified by PCR with FPr1 (5′-GACATTGCTGGCTGGTGATTC) (Fig. 1A) plus RPr2 (5′-GAACAGTG TCCGGTATAGGAGC) (Fig. 1A) or RNeo1 (5′-GAGGATCTCGTCGTGAC CCA) (Fig. 1A). This PCR yielded either a 1.8-kb product indicative of the wild-type allele or a 2.8-kb product indicative of the disrupted or null allele using FPr1 and RPr2 (Fig. 1A) and a 1.8-kb product for the mutant allele using only FPr1 and RNeo1. For faster genotyping on a routine basis, a multiplex PCR assay was designed with FPr3 (5′-AATAGAGCACACATGCCCACAGCC) (Fig. 1A), RPr4 (5′-AAGCACAACATATCCCCAGCAGCC) (Fig. 1A), and FNeo1 (5′-ATAGCCGAATAGCCTCTCCACCCAAG) to yield products of 274 bp for the wild-type allele and 500 bp for the disrupted or null allele (Fig. 1C).

Breeding and superovulation of mice. The significant drop in fertility found upon breeding the CCTβ2 homozygous females with the CCTβ2-deficient males made it necessary to mate the heterozygous females with the knockout males to maintain a breeding colony. Colony littermates were used as female heterozygotes and male wild-type controls, and commercial wild-type female age-matched control mice (129/Sv × C57BL/6J) were purchased from Jackson Laboratory (Bar Harbor, Maine). For ovary maturation and ovulation of immature females, CCTβ2 homozygous and wild-type controls were given intraperitoneal injections of 2.5 U of pregnant mare's serum (Sigma) as a source of follicle-stimulating hormones (FSH) followed by 2.5 U of human chorionic gonadotropin (Sigma) 48 h later (late afternoon) as a source of luteinizing hormone (LH). Females were immediately placed with males and checked for vaginal plugs, indicative of mating, the next morning. Mice were maintained on regular Purina rodent chow #5013 at a room temperature of 72°F ± 2°F, room humidity of 50% ± 10%, and a 12-h light, 12-h dark cycle, with the dark cycle starting at 1800 h. All procedures concerning the care and use of animals were done according to St. Jude Children's Research Hospital Institutional Animal Care and Use Committee approved protocols.

Detection of CCT isoform mRNAs by RT-PCR. Total RNA was isolated from mouse tissues by using TRIZOL reagent according to the manufacturer's instructions. Pelleted RNA was resuspended in nuclease-free water, digested with DNase I to remove any contaminating genomic DNA, aliquoted and reprecipitated in ethanol, and stored at −20°C. Reverse transcription (RT) was done by using SuperScript II RNase H− Reverse Transcriptase (Invitrogen) and the RNA template and random primers to make the corresponding cDNAs. For conventional RT-PCR, multiplex PCR amplification and detection by visual inspection of the CCT cDNAs was performed as described previously (32) by using isoform-specific primers to confirm the absence or presence of expression. Quantitative real-time PCR of the CCT isoforms and PEMT cDNAs was done to measure the relative levels of expression by using the ABI Prism 7700 Sequence Detection System using primers and probes listed in Table 1. The Taqman Rodent GAPDH Control Reagent (Applied Biosystems) was the source of the primers and probe for quantitating the control GAPDH mRNA. RNA was isolated from liver, brain, lung, ovary, and testis of at least three mice of each gender individually, and each RNA sample was quantified in quintuplicate. All of the real-time values for each tissue and gender were averaged and compared by using the C_T method, where the amount of target RNA ($2^{-\Delta\Delta C_T}$) was normalized to the endogenous GAPDH reference (ΔC_T) and related to the amount of target CCTα in liver ($\Delta\Delta C_T$), which was set as the calibrator at 1.0. Standard deviations from the mean ΔC_T values (data not shown) were <10%.

Immunoblotting CCTβ2 protein. Brains from 10-week-old mice were lysed in a Dounce homogenizer and a solution of cold 10 mM Tris-HCl (pH 7.4), 5 mM EDTA, 1 μM Na₃VO₄, 5 mM NaF, 2% aprotinin, 10 μg of leupeptin/ml, 1 mM phenylmethylsulfonyl fluoride. The lysate was centrifuged at 2,000 × g for 20 min at 4°C to remove large debris. Lysate proteins (80 μg) were separated by using NuPAGE 8% gels (Invitrogen) and were electrotransferred to polyvinylidene difluoride membranes. Membranes were washed in a solution of 5% dry milk in 20 mM Tris-HCl (pH 7.4), 137 mM NaCl, 0.1% (vol/vol) Tween-20 (TBS-T) followed by washing in TBS-T alone. Membranes were incubated with 0.5 μg of affinity-purified anti-human CCTβ antibody (32)/ml in 1% dry milk in TBS-T buffer at room temperature for 1 h. The anti-CCTβ antibody cross-reacted with the mouse protein and recognized both CCTβ2 and -β3. Membranes were then washed three times for 15 min each in TBS-T. The ECF Western Blotting kit (Amersham Pharmacia Biotech) was used to detect the primary antibody, and membranes were incubated with the secondary antibody, fluorescein-linked anti-rabbit immunoglobulin G (IgG) diluted 1:600, washed, and then incubated with the tertiary anti-fluorescein antibody conjugated to alkaline phosphatase diluted 1:2,500, according to the manufacturer's instructions. After development of the

TABLE 1. Real-time PCR reagents

Primer	Sequence	Probe
mCCTα-F	5′-TGGATGCACAGAGTTCAGCTAAA	6FAM-CCTCTTTCCTCCTCTTCCTCGAATTGA-TAMRA
mCCTα-R	5′-TGCTCCATTAGGGCCAGGT	
mCCTβ2-F	5′-TTCTTTGCCTGGGAGGAGACT	6FAM-TGCTCCCTCCAGCTCTACACCCT-TAMRA
mCCTβ2-R	5′-AAGTACTGGCATGGCCAGTGA	
mCCTβ3-F	5′-GGGCCAAACCTTGTGGTACA	6FAM-AATTCGTCCTTGTCCATGCTGCAT-TAMRA
mCCTβ3-R	5′-TGCAGTCAGGGTCTTGCGT	
mPEMT-F	5′-GGCATCTGCATCCTGCTTTT	6FAM-CTCCGCTCCCACTGCTTCACAC-TAMRA
mPEMT-R	5′-TTGGGCTGGCTCATCATAGC	

alkaline phosphatase reaction, the immunoblot was scanned by using a Typhoon 9200 Variable Mode Imager (Molecular Dynamics, Amersham Pharmacia Biotech). CCTβ2 (approximately 42 kDa) was distinguished from CCTβ3 (approximately 38 kDa) by its migration distance and comparison with authentic CCTβ2 and CCTβ3 cDNA standards (32).

Tissue histology and fluorescent immunocytochemistry. Mouse tissues were fixed in 10% formalin and processed by dehydration in 70% ethanol, absolute ethanol, and then xylene. Tissues were infiltrated and embedded in paraffin, cut at 4 μm, mounted on microscope slides, and stained with hematoxylin and eosin. For immunocytochemistry, paraffin sections were dewaxed with xylene three times for 3 min each and were rehydrated with 100% ethanol and then 95% ethanol and were then permeabilized with 0.3% Triton X-100 in PBS for 20 min at room temperature. Tissues were blocked with 10% fetal bovine serum (FBS) in PBS for 1 h and rinsed in PBS. Affinity-purified primary antibody (rabbit anti-mouse CCTα [38] or rabbit anti-human CCTβ [35]) or preimmune serum at 10 to 20 ng/ml in 2% FBS in PBS was loaded onto the slices and incubated overnight at room temperature. The next morning, slides were washed three times with PBS, secondary goat anti-rabbit Alexa Fluor 488-labeled IgG (Molecular Probes, Inc.) was applied at a 1:250 dilution in PBS for 1 h at room temperature, and the sections were washed three times with PBS. Sections were mounted in 60% glycerol–1.5% propyl gallate in PBS and sealed with nail polish, and a Nikon E800 microscope was used to examine the tissues for fluorescence.

Serum hormone determinations. Whole blood was collected from mice by orbital bleed or cardiac puncture, allowed to clot at room temperature for 1 h, and centrifuged at $660 \times g$ for 5 min and the clot was removed. The serum was centrifuged again and serum was collected off the top and stored at −80°C until processed for hormone analyses. Serum FSH and LH were measured by the Ligand Assay and Analysis Core Lab, University of Virginia, Charlottesville.

Phospholipid determinations. Flash-frozen brain tissue was thawed and weighed, and approximately 50 mg was extracted by the method of Bligh and Dyer (8). The organic phase containing lipid was concentrated under nitrogen and resuspended in 400 μl of chloroform:methanol (2:1). A 1-μl aliquot was loaded onto a thin-layer silica gel rod and was developed first in ether, dried, and developed in chloroform:methanol:acetic acid:water (50:25:8:3). Lipid mass was detected by flame ionization by using an Iatroscan instrument (Iatron Laboratories, Inc., Tokyo, Japan) with PEAK SIMPLE software (SRI Instruments), and peaks were identified by comigration with authentic standards. PtdCho mass was calculated by using a standard curve prepared with egg PtdCho (Matreya, Inc.).

RESULTS

Quantitative determination of CCT transcripts. We developed quantitative real-time PCR assays to critically evaluate the relative contributions of the different CCTs to PtdCho production in mouse tissues. The PEMT transcripts were also quantified because this enzyme, in addition to the CCTs, mediates a reaction significant for PtdCho biosynthesis in liver tissue (54). This technique has a linear range of more than 4 orders of magnitude which allows for wide-ranging detection of both high and very low copy number transcripts in a sample, and the probe designs are based on a common hybridization condition optimized for all the transcripts. The levels of the transcripts encoding CCTα, CCTβ2, CCTβ3, and PEMT were determined in selected tissues in wild-type 129/Sv × C57BL/6J male and female mice. Both of the CCTα transcripts encode the same protein sequence, and thus the primers were designed to signal both mRNAs. The amounts of target RNA were normalized to GAPDH mRNA and were compared to the level of CCTα in liver (normalized to 1.0) (Fig. 1A). CCTα was most highly expressed in the testis and lung and at lower levels in liver (female) and ovary. The data correlate with the fact that testes and lung secrete large amounts of PtdCho in the seminal fluid and as surfactant, respectively, and the PEMT is expressed at much lower but still significant levels in these organs. On the other hand, liver also has a large capacity for PtdCho production and secretion as a component of the lipoprotein biosynthetic pathway, but the bulk of the PtdCho

synthesis that contributes to lipoproteins is governed in large part by the PEMT, which was expressed at a level about 15 times higher (Fig. 1A and D). The high-density lipoprotein deficiency in choline-deficient PEMT knockout mice (44) is consistent with this view. In comparison, brain did not contain large amounts of either of the CCTs per milligram of tissue weight, and PEMT was almost undetectable despite the fact that the brain is a lipid-rich organ. CCTβ2 and CCTβ3 transcripts, which encode proteins that differ at the amino terminus (32), were consistently expressed together in the same tissues and were most highly expressed in brain, lung, and gonad, although in most cases their levels were at least 10 times lower than the expression level of liver CCTα (Fig. 1B and C). Only in brain did the levels of CCTβ2 and -β3 approach that of CCTα. This was evident when relative levels were compared to one another within individual organs as shown in Fig. 1F. CCTβ2 was at its highest level in brain, where it constituted 30% of the four transcripts (Fig. 1F), whereas CCTβ2 was expressed at a relative value of only about 0.1 compared to that of liver CCTα (Fig. 1A and B). CCTα in the brain constituted about 50% of the four transcripts (Fig. 1F) and was expressed at a value of about 0.17 compared to that of liver CCTα (Fig. 1A). CCTβ2 expression constituted about 30% of the transcripts expressed in female brain, compared to 50% CCTα and 12% PEMT (Fig. 1F). CCTβ2 contributed 5% to the transcript abundance in lung and 1.6% in ovary. These data suggested that the absence of CCTβ2 expression might affect brain or lung most severely.

Deriving CCTβ2-deficient mice. The role of the *Pcyt1b* gene encoding the CCTβ2 protein was investigated by deriving a mouse model that lacked the expression of the full-length CCTβ2 isoform due to disruption of the first coding exon. Genomic clones were isolated and a replacement vector was constructed in which the 3′ end of exon 2 (32) was replaced with the neomycin (*Neo*) resistance gene, and the DTA gene was ligated to the 3′ end of the genomic DNA as a negative selection agent to enrich for homologous recombinants (Fig. 2A). The construct was electroporated into W9.5 ES cells, and several hundred *Neo*-resistant clones were isolated and screened by Southern blotting and PCR as described in Materials and Methods and as illustrated in Fig. 1B. The ES cells were XY; thus, there was only a single X-linked CCTβ (*Pcyt1b*) allele present in the genome, and only a single band on the Southern blots or PCR screens was detected for either the wild-type or recombinant gene (Fig. 2B and C). A clone (#25) where the targeting construct had integrated by homologous recombination into the CCTβ gene was identified, and a normal karyotype (*n* = 40) was confirmed. Clone 25 was injected into C57BL/6J blastocysts and was implanted into pseudopregnant F_1 B6/CBA foster mothers at the St. Jude Transgenic Core Facility. Male chimeras (129/Sv × C57BL/6J) were bred with C57BL/6J females, and the F_1 agouti pups that arose from germ line transmission of the disrupted CCTβ2 allele as determined by Southern blot analysis were interbred to generate F_2 animals for genotyping (as shown in Fig. 2C) and subsequent study. Female mice with the CCTβ2$^{-/-}$ genotype (25%) and male mice with the CCTβ2$^{-/0}$ genotype (25%) were routinely obtained in the litters derived from breeding the +/− × −/0 animals, indicating that there was no fetal death of the homozygous knockout animals. However, a reproductive de-
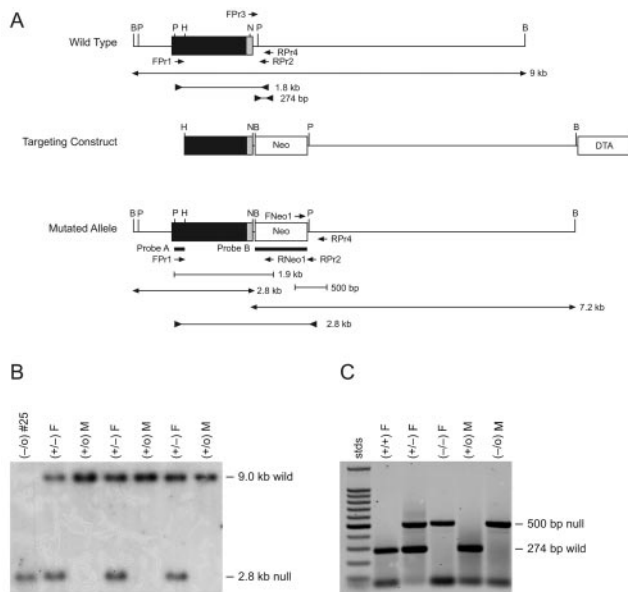
FIG. 2. CCTβ2 targeting construct and analysis of the knockout mouse genotypes. (A) The 9-kb BamHI wild-type genomic clone was obtained from library screening as described in Materials and Methods. The black box indicates the extent of exon 2, and the gray zone is the coding portion of the exon. The targeting construct inserts the *Neo* resistance gene into exon 2 at the NcoI site, eliminating part of the CCTβ2 coding sequence. The DTA gene was inserted at one end of the vector for counterselection of recombinant clones. The structure of the mutated allele after the integration of the *Neo* gene by homologous recombination is shown on the last line. Probes A and B were used for Southern blotting, which detected the bands with outward-pointing arrows. Bands detected by PCR as described in Materials and Methods are indicated by the inward-pointing arrows. Restriction enzymes are abbreviated as follows: B, BamHI; P, PstI; H, HindIII; and N, NcoI. (B) An example of Southern blot analysis of mouse genomic DNA. Genomic DNA was isolated and digested with BamHI, and the fragments were separated by agarose gel electrophoresis. The blot was probed with ^{32}P-labeled probe A, a PstI-HindIII fragment located outside of the targeting construct. The wild-type allele is revealed by hybridization with a 9-kb band, whereas the mutant allele gives a 2.8-kb band due to the presence of a new BamHI site within the inserted *Neo* gene. Sample #25 is the ES cell clone used for the blastocyst injections. Probe B was used in Southern blot experiments to detect the presence of the 7.2-kb *Neo* gene fragment in the BamHI digest to confirm the genotype of the mice (data not shown). (C) An example of the PCR analysis used to genotype mice. A multiplex PCR consisting of a mixture of primers FPr3, FNeo1, and RPr4 were used to signal either the 274-bp wild-type allele or the 500-bp null allele. PCRs used to screen the ES cell clones consisted of FPr1 coupled with RPr2 or RNeo1 to give a 1.8-kb band in the wild-type cells and a 2.8-kb band in the mutant cells (data not shown).

fect in the CCTβ2-deficient animals (see below) precluded the establishment of a homozygous breeding colony, and routine mating of heterozygotes and genotyping of the pups was necessary to propagate the CCTβ2$^{-/-}$ mice.

CCT isoform expression in knockout mice. The expression, or lack thereof, of CCTβ2 was confirmed in the mouse pups by performing conventional RT-PCR analysis of the RNA from selected organs from the wild-type and knockout animals. These experiments also addressed whether expression from the CCTβ3 exon 1 lurking 18.5 kb upstream would be affected by the insertion of the *Neo* gene into exon 2. At the same time, we surveyed the expression of both of the CCTα transcripts, α1
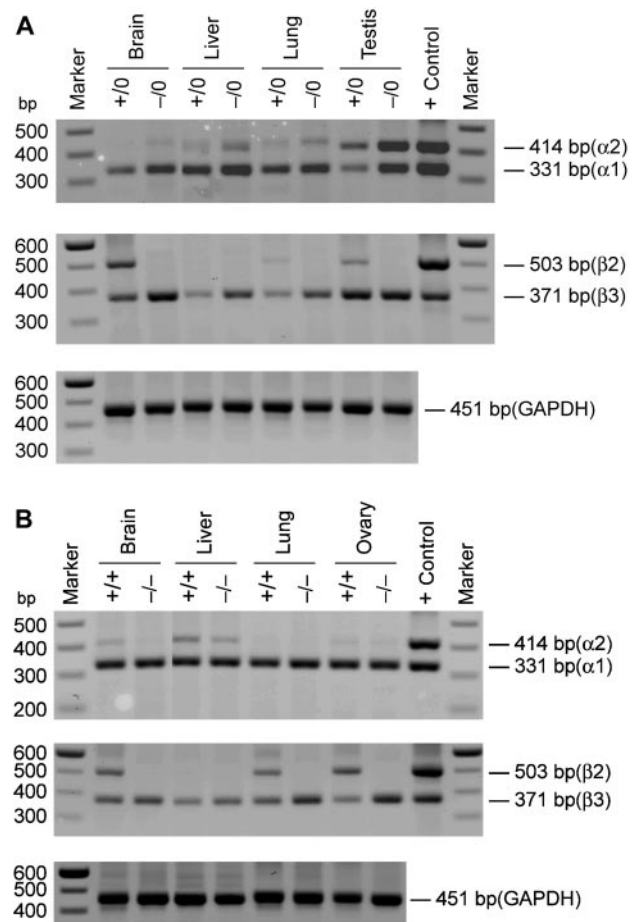

FIG. 3. Expression of CCTα and CCTβ mRNAs in tissues from male and female wild-type and CCTβ2-deficient mice. Tissues were removed from male (A) and female (B) animals with the indicated genotypes, RNA was isolated, and the samples (10 μg) were screened by using multiplex PCR to detect the two CCTα and two CCTβ mRNAs as described in Materials and Methods. The CCTα1 mRNA was detected as a 331-bp product, and CCTα2 was a 414-bp product. The presence of CCTβ2 was detected by a 503-bp band, and CCTβ3 yielded a 331-bp product. The control primer pair signaled a 451-bp fragment of the GAPDH mRNA.

and α2, arising from the alternate gene *Pcyt1a* (Fig. 3). The CCTβ transcripts were detected visually after 40 cycles of PCR, whereas detection of CCTα transcripts required only 30 cycles, confirming our results from the real-time PCR measurements that CCTβ was expressed at a much lower level in most mouse tissues. Male CCTβ2$^{-/0}$ mice showed the expected distribution of CCTα expression (Fig. 3A) (32), which included the unique expression of CCTα2 in the testis. All male CCTβ2$^{-/0}$ tissues lacked the expression of the CCTβ2 transcript but retained CCTβ3 expression. The same general pattern was true in the female CCTβ2$^{-/-}$ mice (Fig. 3B), which expressed CCTα1, CCTα2, and CCTβ3 transcripts as detected by this methodology. These data established that the expression of the full-length CCTβ2 transcript was abolished in both the male and female knockout mice.

Because CCTβ2 was most highly expressed in brain tissue, we confirmed that the full-length CCTβ2 protein was present in wild-type brains and that it was absent in the CCTβ2$^{-/-}$
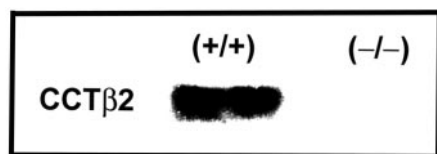
FIG. 4. Immunoblot analysis of CCTβ2 protein expression. Western blotting was performed by using mouse brain tissue. Wild-type (+/+) and knockout (−/−) female brains were homogenized and separated on 8% NuPAGE gels prior to blotting with a CCTβ isoform-specific antibody (32). CCTβ2 migrates at a molecular size of 42 kDa.

brains by immunoblotting tissue homogenates with a CCTβ isoform-specific antibody (Fig. 4). However, measurements of brain PtdCho (in micrograms per milligrams of weight) did not reveal a significant difference between wild-type 129/Sv × C57BL/6J mice (18.97 ± 3.69, $n = 24$) and knockout mice (18.73 ± 2.36, $n = 24$). Our results suggested that there may be excess capacity for PtdCho synthesis, represented by the copy number of the rate-controlling enzymes in brain (and other tissues), and the loss of about one-third of the CCT transcripts does not have a gross effect.

We were somewhat surprised that disruption of CCTβ2 expression in mice did not have any overt effect brain development, content, or morphology in light of recent reports that CCTβ2 expression was selectively upregulated in the hippocampus by the neuropeptide arginine-vasopressin$_{(4-8)}$ (63) and during neurite outgrowth of NGF-treated PC12 cells (12). We addressed this inconsistency by using our real-time PCR tools to quantify the changes in the CCT transcript levels in PC12 cells stimulated with NGF to determine whether the information obtained by using an immortalized cell line was distinctly different from that obtained from the whole animal. PC12 cells respond to NGF by ceasing cell division and extending neurite-like outgrowths associated with a fourfold increase in the total protein per cell (23). In our experiments, NGF-treated PC12 cells exhibited neurite outgrowth and the total protein increased from 796.2 μg per 10^7 cells to 2,168.7 μg per 10^7 cells following addition of 100 ng of NGF/ml to the cultures for 5 days. The amount of protein and the amount of total RNA per dish was equivalent for comparisons of NGF-treated and untreated cells cultured for 5 days. However, the cell number of the NGF-treated cultures was significantly lower (2.6 × 10^7 cells in untreated 100-mm-diameter dishes compared to 0.83 × 10^7 cells in those exposed to NGF), consistent with the known functions of NGF to halt proliferation, trigger the differentiation, and support survival of PC12 cells (22, 23, 50). Whereas the relative amount of CCTβ2 transcript per cell increased by a factor of 3.8, from 0.268 to 1.02 in our measurements, in agreement with the previous report (12), the amount of CCTα transcript per cell also increased, from 1.0 to 2.48 (Fig. 5A). We also quantified the CCT transcript levels normalized to total RNA, and the relative amounts of CCTα and CCTβ2 transcripts were not significantly different in control and NGF-treated cells. The ratio of CCTα to CCTβ2 transcript was about 3.7 to 1 in undifferentiated PC12 cells and was 2.5 to 1 in PC12 cells treated with NGF (Fig. 4), in general agreement with our data for primary brain tissue, where there was approximately a 2:1 ratio of CCTα and CCTβ2 and -β3 expression (Fig. 1F). CCTβ3 was found not to be expressed in
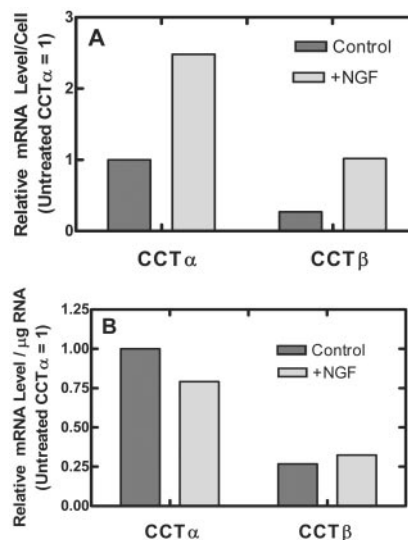

FIG. 5. CCT expression in PC12 cells. PC12 cells were cultured with NGF (100 ng/ml) or alone for 5 days in duplicate 100-mm-diameter dishes in two independent experiments. Total RNA was isolated from each culture and quantified, and the relative amounts of CCTα, CCTβ2, and CCTβ3 transcripts per microgram of RNA were determined in quintuplicate by using real-time PCR as described in Materials and Methods. The amount of target RNA ($2^{-\Delta\Delta CT}$) was normalized to the endogenous GAPDH reference (ΔC_T) and was related to the amount of target CCTα in untreated control cultures ($\Delta\Delta C_T$), which was set as the calibrator at 1.0. The averages of three sets of determinations are reported for CCTα, and the averages of two sets of determinations are reported for CCTβ2 and CCTβ3. Standard deviations from the mean ΔC_T values (not shown) were <10%. Cell numbers and protein determinations were measured by using duplicate parallel cultures. (A) Data normalized to number of cells; (B) data normalized to micrograms of total RNA.

the PC12 cells in both labs. Therefore, these data point out an increase in CCTα expression as well as CCTβ2 expression upon neuronal differentiation and are consistent with our CCT expression results for mouse brain. These data also support the view that sufficient CCTα is present in the brain to support cellular and tissue function and structure in the absence of CCTβ2.

We investigated whether there were compensatory changes in CCT expression to explain normal organ development and function in CCTβ2-deficient mice. Previously in mice where CCTα expression was eliminated in macrophages, the cells survived due to an upregulation of CCTβ2 expression (66). There was no change in the CCTα, CCTβ3, or PEMT transcript levels in liver, brain, or gonads of the knockout CCTβ2 mice (data not shown). However, in lung there was a 28% increase in CCTα expression in the male and about a 50% increase in the female CCTβ2-deficient mice. The result was selective for CCTα, as the PEMT transcripts which constituted a small but significant portion of those surveyed in lung did not change. The amount of CCTβ3 transcript also did not change (data not shown). The reason for this apparent upregulation of CCTα expression in the lungs of CCTβ2 knockout animals is not clear.

Reproductive phenotype of the CCTβ2-deficient mice. Heterozygous CCTβ2$^{+/−}$ females were mated with CCTβ2$^{−/0}$ males, and the CCTβ2$^{−/−}$ female pups appeared outwardly
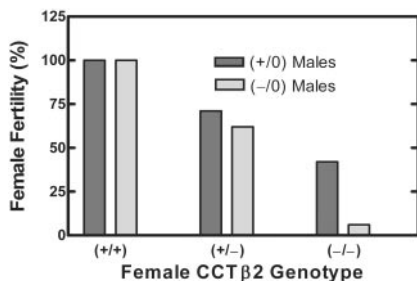
FIG. 6. Fertility of CCTβ2$^{-/-}$ females. Female mice (2 to 4 months old) with the indicated genotypes were paired 1:1 with either wild-type or CCTβ2$^{-/0}$ males as indicated for 2 months and were scored as fertile if they were pregnant or had borne pups at least once by the end of that time period. Comparison of the mating groups was done by the Fisher exact test. For CCTβ2$^{+/+}$ × CCTβ2$^{+/0}$ ($n = 27$) compared to CCTβ2$^{-/-}$ × CCTβ2$^{+/0}$ ($n = 19$), $P < 0.001$; for CCTβ2$^{-/-}$ × CCTβ2$^{+/0}$ ($n = 19$) compared to CCTβ2$^{-/-}$ × CCTβ2$^{-/0}$ ($n = 16$), $P = 0.022$; for CCTβ2$^{+/+}$ × CCTβ2$^{-/0}$ ($n = 6$) compared to CCTβ2$^{-/-}$ × CCTβ2$^{-/0}$ ($n = 16$), $P < 0.001$; for CCTβ2$^{+/+}$ × CCTβ2$^{+/0}$ or CCTβ2$^{-/0}$ ($n = 30$) compared to CCTβ2$^{+/-}$ × CCTβ2$^{+/0}$ or CCTβ2$^{-/0}$ ($n = 36$), $P < 0.001$.

normal. However, the adult homozygous CCTβ2$^{-/-}$ females had reduced numbers of pregnancies. CCTβ2$^{-/-}$ females delivered normal numbers of pups per litter (8.3 ± 2.4, $n = 22$) compared to the wild-type 129/Sv × C57BL/6J females (7.7 ± 2.3, $n = 14$), and the female and male pups in both groups were average weight (CCTβ2$^{+/+}$ mice, 17.3 ± 0.9 g, $n = 10$; CCTβ2$^{-/-}$ mice, 17.8 ± 0.85 g, $n = 7$; CCTβ2$^{+/0}$ mice, 19.9 ± 1.4 g, $n = 8$; CCTβ2$^{-/0}$ mice, 19.7 ± 0.7, $n = 10$ at 5 weeks). A study was done where 1:1 mating pairs of homozygous, heterozygous, and wild-type virgin mice between the ages of 2 and 4 months were maintained together for 2 months and the females were scored as fertile or barren. The data in Fig. 6 report the percentages of mature females who had at least one litter. Those mice which were scored as barren did not show evidence of pregnancy. Less than 50% of the homozygous CCTβ2$^{-/-}$ females were fertile when mated with wild-type 129/Sv × C57BL/6J males ($P < 0.001$ compared to wild-type females), and fertility decreased when the CCTβ2-deficient females were matched with knockout CCTβ2$^{-/0}$ males ($P < 0.001$) (Fig. 6). The percentage of heterozygous females mated to either wild-type or knockout males and that birthed pups was also reduced significantly ($P < 0.001$) (Fig. 6). Keeping in mind that the *Pcyt1b* gene is located on the X chromosome, this result may have been due to random X inactivation of the single wild-type allele which would occur with about a 50% frequency, conferring a knockout phenotype on the heterozygous females with two effectively dysfunctional alleles. Alternatively, the lower pregnancy percentage of the heterozygous females could have been due to a gene dosage effect. There was a significant drop ($P < 0.022$) in female pregnancy when the CCTβ2 homozygous knockout females were bred with CCTβ2-deficient males compared to results for breeding with wild-type males, suggesting a reproductive defect in the male knockout mice as well (Fig. 6). Tissue samples were obtained from the 4- to 6-month-old females and males in this study for histological analysis (see below).

Ovary pathology in CCTβ2$^{-/-}$ knockout females. An explanation for the reduced fecundity in the groups of CCTβ2$^{-/-}$

and CCTβ2$^{+/-}$ females was evident from microscopic examination of the ovaries. Ovaries from a 4-month-old wild-type mouse and a knockout mouse are shown in Fig. 7. The wild-type ovaries exhibited normal ovary morphology with developing follicles and multiple corpora lutea. Higher magnification revealed highly organized germinal epithelial cells and interstitial stromal cells and follicles at several stages of development with ova. However, the infertile CCTβ2$^{-/-}$ mice had no follicles or corpora lutea. Higher magnification revealed epithelial and interstitial stromal cell hyperplasia, with invagination of the epithelial cells into the interstitial stromal cell layer forming epithelial tubules and cords of interstitial stromal cells. Fertile CCTβ2$^{-/-}$ mice, on the other hand, had ovaries with normal morphologies. The ovaries of a subset of the heterozygous females ($n = 10$) were also examined, and 40% exhibited aberrant ovarian morphology, with the absence of follicles and corpora lutea. Those mice with the abnormal ovarian pathology were also barren. The data support the idea that the reproductive defect in CCTβ2-deficient females was due to a failure in ovary maturation.

We compared ovarian pathologies as a function of age. At 4 weeks, 89% of knockout virgin females had normal ovaries ($n = 9$); 45% of the animals between 2 to 5 months of age were normal ($n = 17$), at 6 months 38% were normal ($n = 8$), and at 16 months 17% of the ovaries were normal ($n = 6$). Examination of wild-type 129/Sv × C57BL/6J ovaries on multiple occasions between ages 4 weeks to 6 months showed 100% normal ovaries. In a separate study, when immature 4-week-old CCTβ2$^{-/-}$ female mice were treated with FSH and LH to induce follicle maturation and ovulation and then were mated for 1 month, 3 out of 10 were fertile compared to age-matched treated wild-type 129/Sv × C57BL/6J females, all of which successfully became pregnant (100%, $n = 10$). These data suggested that that ovary dysfunction and infertility preceded the overt pathology of the defective ovaries in the younger CCTβ2$^{-/-}$ females and that the ovaries of an increasing percentage of females were not able to develop follicles as the animals aged. The abnormal ovaries from the 16-month-old CCTβ2 knockout females had infiltrating tubulostromal tumors (Fig. 8). The tumor cells were similar to the epithelial and interstitial stromal cells of the ovaries of the CCTβ2$^{-/-}$ females, but the tumor cells invaded the adipose tissue of the ovary's hilus. Although the tumor cells were invasive, their cytological morphology was benign and mitotic figures were not evident. We concluded from these results that long-term absence of CCTβ2 expression in ovarian tissue resulted in the development of benign ovarian tumors. The older CCTβ2$^{-/-}$ tumors varied in their proportion of epithelial and interstitial stromal cell components, and occasionally there were foci of granulosa cells.

The serum FSH and LH levels of 4-month-old mice were investigated and correlated with ovarian morphologies. We found a 100% correlation between aberrant ovarian pathology and elevated FSH and LH levels. Wild-type and CCTβ2-deficient animals with normal ovaries had average serum FSH values (± standard error) of 7.1 ± 0.5 ng/ml and LH of 0.4 ± 0.05 ng/ml ($n = 40$), whereas the CCTβ2$^{-/-}$ animals with ovaries that lacked follicles or corpora lutea had significantly higher FSH values of 63.7 ± 3.4 ng/ml ($P < 0.0001$) and LH values of 5.5 ± 1.2 ng/ml ($P < 0.0001$) ($n = 10$). Occasionally
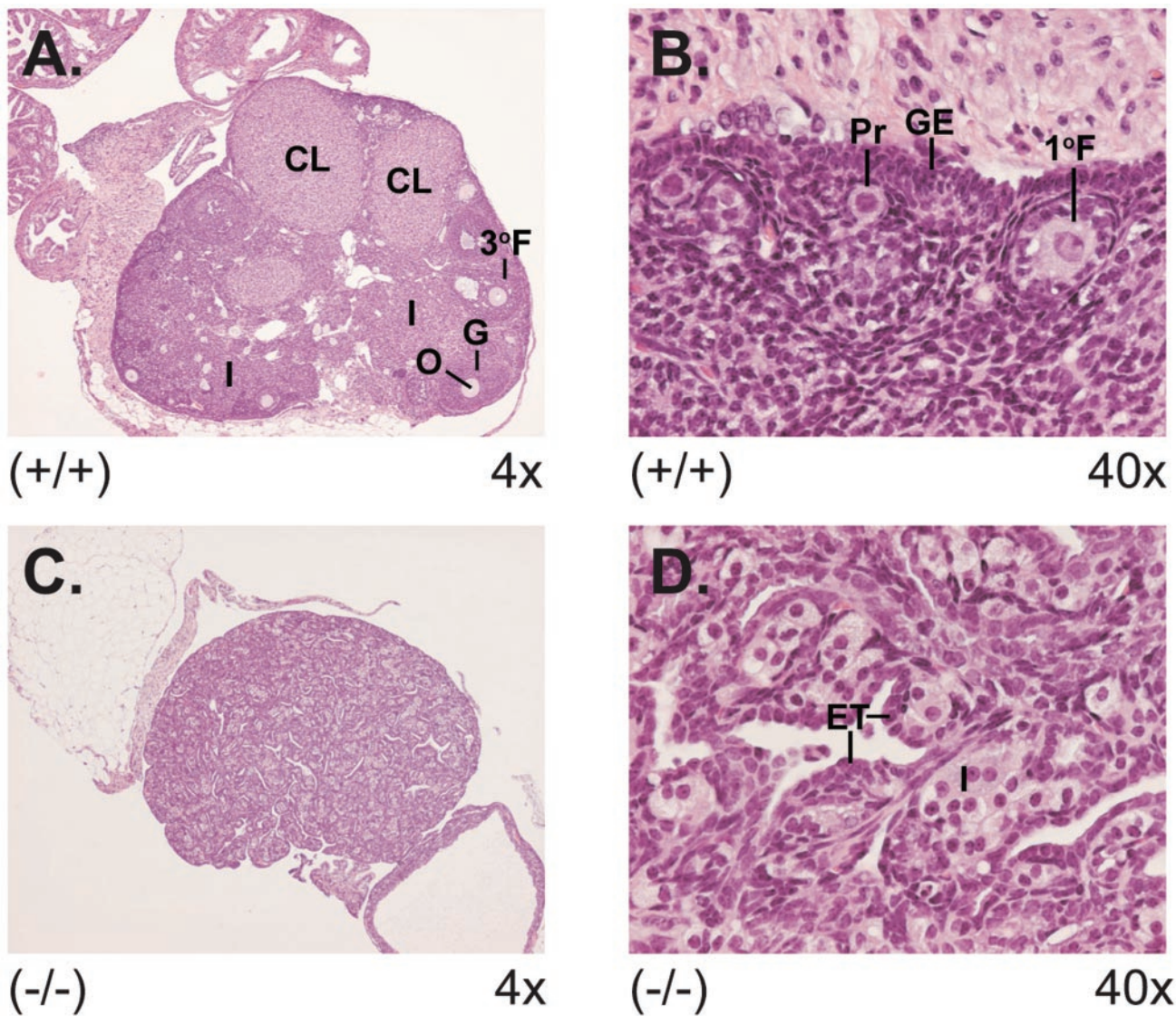
FIG. 7. Aberrant ovary morphology in CCTβ2$^{-/-}$ mice. The ovaries from wild-type and CCTβ2$^{-/-}$ knockout mice were removed, fixed, and stained for pathology analysis. (A) View (magnification, ×4) of a normal ovary showing developing follicles and multiple corpora lutea. Structures indicated are the following: 3°F, tertiary follicle with ovum; O, ovum; G, granulosa cells; CL, corpus luteum; and I, interstitial stromal tissue. (B) View (magnification, ×40) of a normal ovary showing the following: Pr, primordial follicle with ovum; 1°F, a primary follicle with ovum surrounded by a layer of granulosa cells; and GE, organized germinal epithelial cell layer. (C) View (magnification, ×4) of a CCTβ2$^{-/-}$ knockout ovary illustrating the absence of ova, follicles, and corpora lutea. (D) View (magnification, ×40) of a CCTβ2$^{-/-}$ ovary showing hyperplastic epithelial cells, invaginating into and dissecting the interstitial stromal cell tissue forming epithelial tubules (ET) and cords of interstitial stromal cells with foamy cytoplasm (I).

an ovary from either a CCTβ2$^{-/-}$ or CCTβ2$^{-/+}$ female would exhibit evidence of follicles along with hyperplasia of the interstitial stromal cells, and the FSH levels in these cases were midrange.

Testis pathology and serum hormone levels in CCTβ2$^{-/0}$ males. An explanation for the reduced fertility of the CCTβ2$^{-/0}$ males (Fig. 6) was evident from microscopic examination of the testes from the 4- to 6-month-old mice. A testis from a 6-month-old CCTβ2$^{-/0}$ male is shown in Fig. 8. Wild-type testes exhibited normal organization of seminiferous tubules with spermatogenesis, mature sperm, and tubular interstitial Leydig cells (Fig. 9A and B). Testes from CCTβ2-deficient mice showed seminiferous tubular degeneration at multiple

foci and reduced spermatogenesis (Fig. 9C and D). The number of animals with abnormal testicular pathology and the severity of testicular degeneration increased with age. Two- to 4-month-old CCTβ2-deficient males exhibited mild seminiferous tubular degeneration (58%, $n = 12$), while at 6 months 71% showed severe multifocal seminiferous tubular degeneration ($n = 7$ animals). These data are consistent with the reduced fertility seen with the CCTβ2$^{-/0}$ males (Fig. 6). The fact that successful insemination by males can still occur in animals with lower than normal sperm production explains why the male reproductive defect was not as obvious until the males aged. In contrast with the CCTβ2$^{-/-}$ females, the aberrant testis morphology of the CCTβ2-deficient males was not ac-
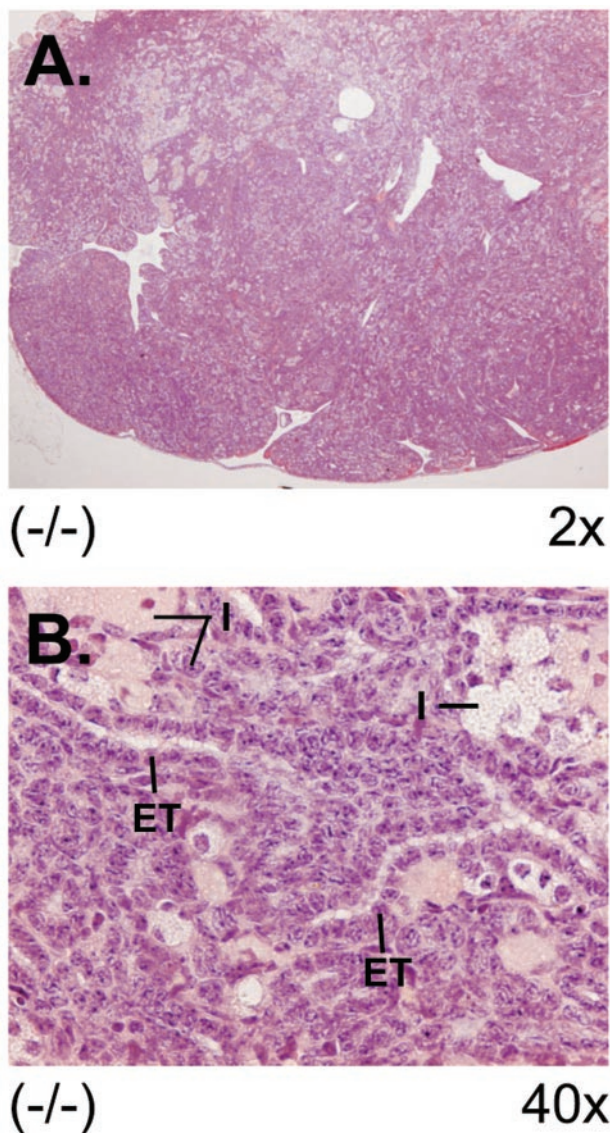
FIG. 8. Ovarian tumor derived from an aged CCTβ2$^{-/-}$ mouse. (A) View (magnification, ×2) of an ovary from age 16 months, showing epithelial, tubular, and interstitial components of tubulostromal tumor lacking ova, follicles, or corpora lutea. (B) View (magnification, ×40) of the tumor showing disorganized morphology with epithelial tubules (ET) and interstitial stromal cells with eosinophilic, foamy, or brown-gold cytoplasm dispersed between the tubules (I).

bule degeneration, diffuse interstitial Leydig cell hyperplasia was noted in the 16-month-old males.

CCT protein expression in gonadal tissues. The CCT isoform distributions were determined in gonadal tissue from wild-type 129/Sv × C57BL/6J female and male mice by using anti-CCTα and anti-CCTβ antibodies for immunofluorescent cytochemistry. The CCTα affinity-purified antibody was raised against a peptide located at the amino terminus of the mouse protein. The CCTβ affinity-purified antibody was raised against a peptide located at the carboxy terminus of the human protein (35) and cross-reacted with the rodent protein (32), and it recognized both the β2 and β3 isoforms (32). As negative controls for nonspecific staining, preimmune serum at the same protein concentration was used, and the fluorescent signal from this preparation was not detectable at the same exposure. As shown in Fig. 10, CCTα was expressed throughout the ovary, including granulosa cells and ova, and at high levels in interstitial stromal cells (Fig. 10B). CCTβ proteins, in contrast, were present at comparatively lower levels in the ovary but with high staining in mature ova (Fig. 10C). In knockout females, CCTα was present throughout the tissue at the same level of staining and the CCTβ staining of the ova appeared to be reduced relative to the signal in the wild-type ovary (data not shown). These data suggested that CCTβ2 expression in the normal ovary was highest in ova, although CCTα and -β3 were also present. CCTα and CCTβ protein expression was evident throughout wild-type testicular tissue, with the CCTβ immunofluorescence of the interstitial Leydig cells being less intense than the seminiferous tubule germinal cells (Fig. 11B and C). The cellular staining pattern of the knockout testes did not change dramatically outside of the rearrangement of the tissue architecture (data not shown). The reactivity of both CCTβ2 and CCTβ3 with the CCTβ antibody precluded a clear designation of a cell-specific role for only CCTβ2 in gonadal tissues. Nonetheless, these data showed CCT protein expression in all of the gonadal cells, with preferential CCTβ distribution in maturing ova and less CCTβ expression in the interstitial Leydig cells of the testis.

DISCUSSION

Deletion of CCTβ2 expression in mice revealed an essential role for this isoform in ovary maturation and the maintenance of sperm production. Considering the low level of CCTβ2 expression in gonads that was revealed by quantitative real-time PCR, it is remarkable that the animals have a gonadal phenotype. It would be virtually impossible to link a biochemical defect in PtdCho metabolite distribution to the loss of CCTβ2 expression due to the very low expression level of CCTβ2 compared to that of CCTα, which is expressed at a 20-fold higher level in ovaries and a 350-fold higher level in testes (Fig. 1). CCTβ3 is also expressed in the CCTβ2-deficient animals and probably performs the same cellular function as CCTβ2 due to its nearly identical protein sequence. The challenge of repeated maturation of the gametes during adulthood accompanied by successive rounds of cellular differentiation may have allowed the phenotypic deficiency to be revealed.

Animals had reduced fertility due to defective ovarian follicular development and testicular spermatogenesis. Postnatal ovarian follicles were evident, as were testicular spermatogo-
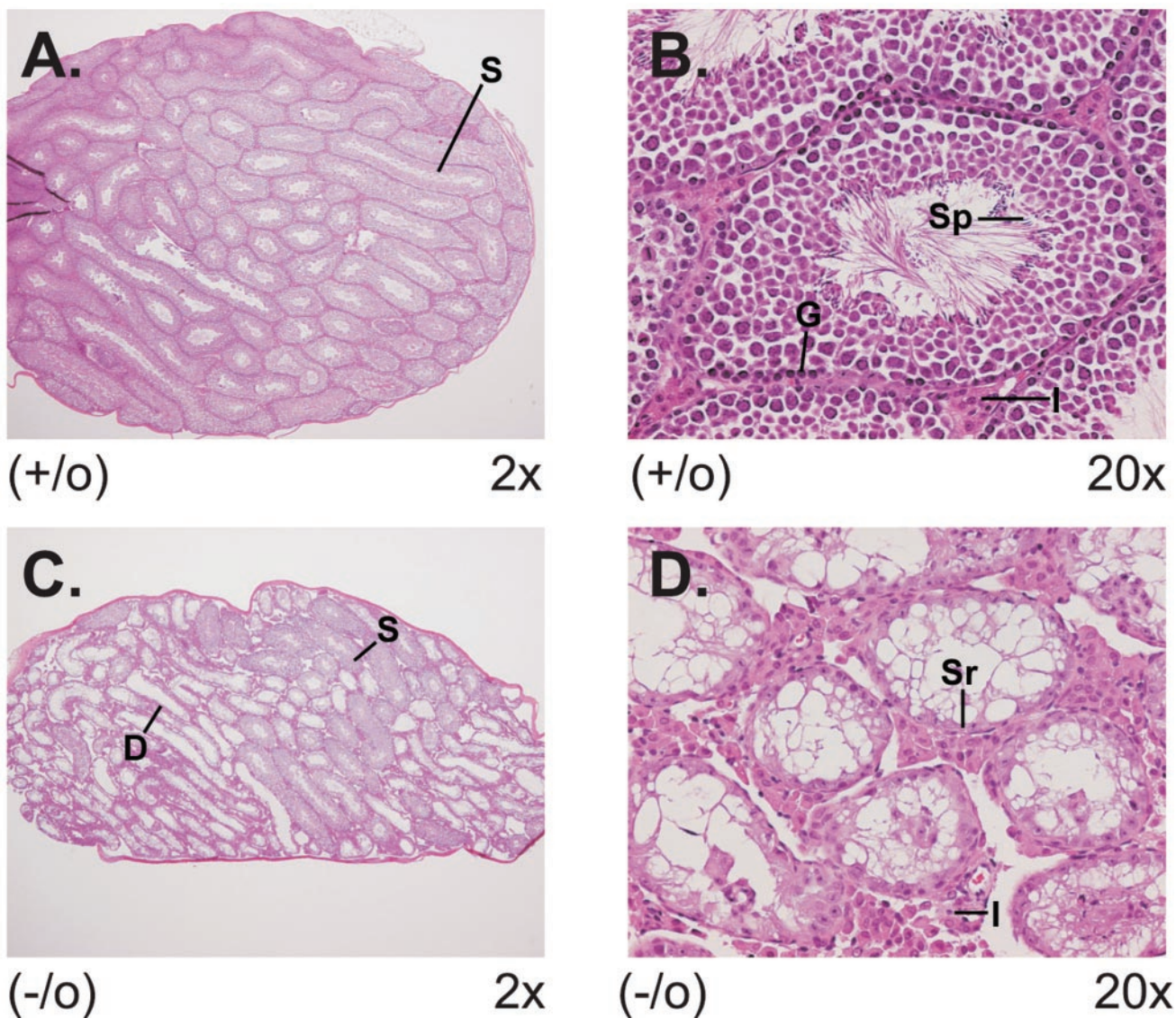
companied by significantly increased FSH (40.2 ± 6.9 ng/ml, n = 7) or LH (0.2 ± 0.2 ng/ml, n = 7) values at 2 months or at 6 months (FSH, 51.3 ± 14.5 ng/ml, n = 7; LH, 0.9 ± 1.5 ng/ml, n = 7) compared to those of age-matched, wild-type littermate controls (for 2-month-old mice, FSH was 33.6 ± 7.8 ng/ml, P = 0.134, n = 7; for 6-month-old mice, FSH was 55.4 ± 9.7 ng/ml, P = 0.57, n = 6; for 2-month-old mice, LH was 0.1 ± 0.1 ng/ml, P = 0.26, n = 7; for 6-month-old mice, LH was 0.4 ± 0.6 ng/ml, P = 0.46, n = 6). At age 16 months, the testes of CCTβ2-deficient males (100%, n = 6) were atrophic compared to those of wild-type littermate controls and, in contrast with the ovaries from CCTβ2-deficient females, did not show evidence of testicular tumors. However, in addition to seminiferous tu-

FIG. 9. Aberrant testis morphology in CCTβ2$^{-/0}$ mice. The testes from 6-month-old CCTβ2$^{-/0}$ knockout mice and wild-type littermate controls were removed, fixed, and stained for pathology analysis. (A) View (magnification, ×2) of a wild-type testis showing seminiferous tubules with small lumens (S). (B) View (magnification, ×20) of testis showing seminiferous tubules with 4 to 5 germinal cell layers composed of spermatogonia and Sertoli cells and spermatogenesis progressing from the basal germinal layer (G) to mature spermatids (S) with their tails extending into the lumen. Interstitial Leydig cells (I) are located in the space between the seminiferous tubules. (C) View (magnification, ×2) of a CCTβ2$^{-/0}$ knockout testis illustrating multiple foci of degenerate seminiferous tubules with a large lumen (D) and also normal seminiferous tubules with a small lumen (S). (D) View (magnification, ×20) of a CCTβ2$^{-/0}$ knockout testis showing multiple small degenerative seminiferous tubules with reduced number of germinal cell layers and absence of spermatozoa. Sertoli cells (Sr) are the predominant cells associated with the basal germinal layer, and interstitial Leydig cells (I) are increased between the tubules.

nia, Sertoli cells, and interstitial Leydig cells in CCTβ2 knockout weanling animals, and both tissues arise from the same embryonic origin (25), suggesting that CCTβ2 is not necessary for the embryonic development of the gonads. However, a large percentage of the older female mice that lacked CCTβ2 expression were unable to develop mature ovarian follicles, and CCTβ2-deficient testes became progressively atrophic with reduced spermatogenesis. Follicle and oocyte maturation, as well as testicular stem cell renewal and differentiation into Sertoli cells and spermatids, occur in response to circulating pituitary hormonal stimuli in mature animals. However, the gonadal problems did not arise from deficient reproductive

hormone production from the pituitary. The high levels of FSH and LH in the CCTβ2$^{-/-}$ females with abnormal ovaries coupled with the lack of elevated FSH and LH levels in the CCTβ2$^{-/0}$ males with degenerating testes argue that the pituitary gland is capable of synthesizing and secreting ample amounts of the reproductive hormones. The lack of a growth defect in the CCTβ2-deficient mice is consistent with sufficient secretion of growth hormone, another pituitary product, and microscopic examination of brain slices through the hypothalamic-pituitary axis did not reveal alterations in aged knockout animals (data not shown). Thus, the reproductive defect probably arises from a unique requirement for CCTβ2 activity in
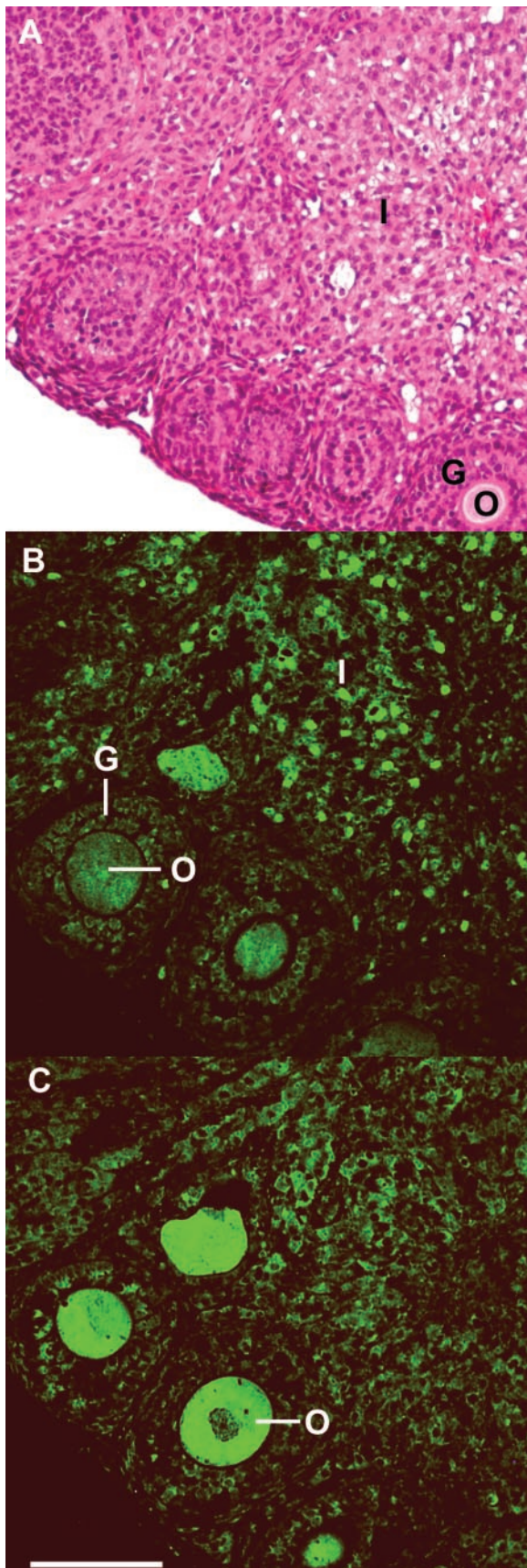
the gonads, where the CCTβ2 protein functions in a pathway critical to maintaining the repeated germ cell differentiation that takes place in the gonads after puberty and through adulthood. CCTβ3 is still expressed in the knockout mice and is governed by a different promoter (32); therefore, the loss of response of the ovary and testis to stimulatory ligands or growth factors may be due to total CCTβ expression falling below a threshold level.

There are several signaling pathways that are essential for normal ovary maturation and maintenance. Development of the gonads after birth is dependent on FSH and LH production by the pituitary gland and on the production of steroid hormones in the testis and ovary (33, 61). Gonad maturation is also dependent on growth factors as shown in mice with mutations at the *white-spotting (W)*, *steel (Sl)*, or deficiency in growth differentiation factor 9 (*Gdf9*) loci or sheep with the FecX (Inverdale) defect (9, 11), which all have reduced fertility due to the absence of normal ovarian follicle development followed by ovarian degeneration. Mice with the *W/W* defect also develop ovarian tumors (1). The *W* gene encodes the c-*kit* growth factor receptor (13, 43), which is expressed in growing oocytes as well as other cell types, and the *Sl* (steel) locus encodes the ligand for the c-*kit* receptor and is expressed in follicle cells (26, 67). Mice with homozygous mutations in either locus lack germ cells, and their ovaries develop to the stage when germ cells would enter meiosis but have arrested differentiation (41, 42). GDF-9 (also known as FecX) is an oocyte-derived growth factor required for ovarian somatic cell function (21, 39, 62). Similar to the CCTβ2$^{-/-}$ mice, ovarian degeneration or regression in animals with these mutant alleles is associated with significantly elevated serum FSH and LH (39, 49).

CCTα is the dominant isoform (Fig. 1) and is expressed in virtually all gonadal cells (Fig. 10), although its highest level occurs in the nuclei of the interstitial stromal cells (Fig. 10). These cells produce progesterone, providing an essential step in female cycling. The immunocytochemistry also reveals that CCTβ2 is a major determinant of PtdCho synthesis in wild-type maturing ova (Fig. 10). CCTβ2$^{-/-}$ ovaries have staining, indicating that CCTβ3 is still expressed in the ova and suggesting that disruption of both β2 and β3 expression might yield a completely infertile female phenotype. There is an intimate relationship between ova and granulosa cells that is essential to the maturing follicle illustrated by the research on GDF-9 (40), and epidermal growth factor (EGF)-like receptors are critical mediators of LH action in ovaries (46). One interpretation of our data is that CCTβ2-mediated PtdCho synthesis may be required to support the paracrine stimulation between these

FIG. 10. Fluorescent immunocytochemistry of CCT expression in ovary. Wild-type C57BL/6J × 129J ovary (age, 4 months) was fixed and stained with hematoxylin and eosin (A), rabbit anti-mouse CCTα antibody (B), or rabbit anti-human CCTβ antibody (C), followed by goat anti-rabbit Alexa Fluor 488-coupled secondary IgG (H + L). Substitution of preimmune rabbit serum for the primary antibody did not yield a fluorescent image at the same exposure. Structures indicated are the following: I, interstitial stromal cells; O, ova; and G, granulosa cells. CCTα is most highly expressed in the nuclei of the interstitial stromal cells (B), whereas CCTβ is more highly expressed in the ova (C). Scale bar, 0.1 mm.
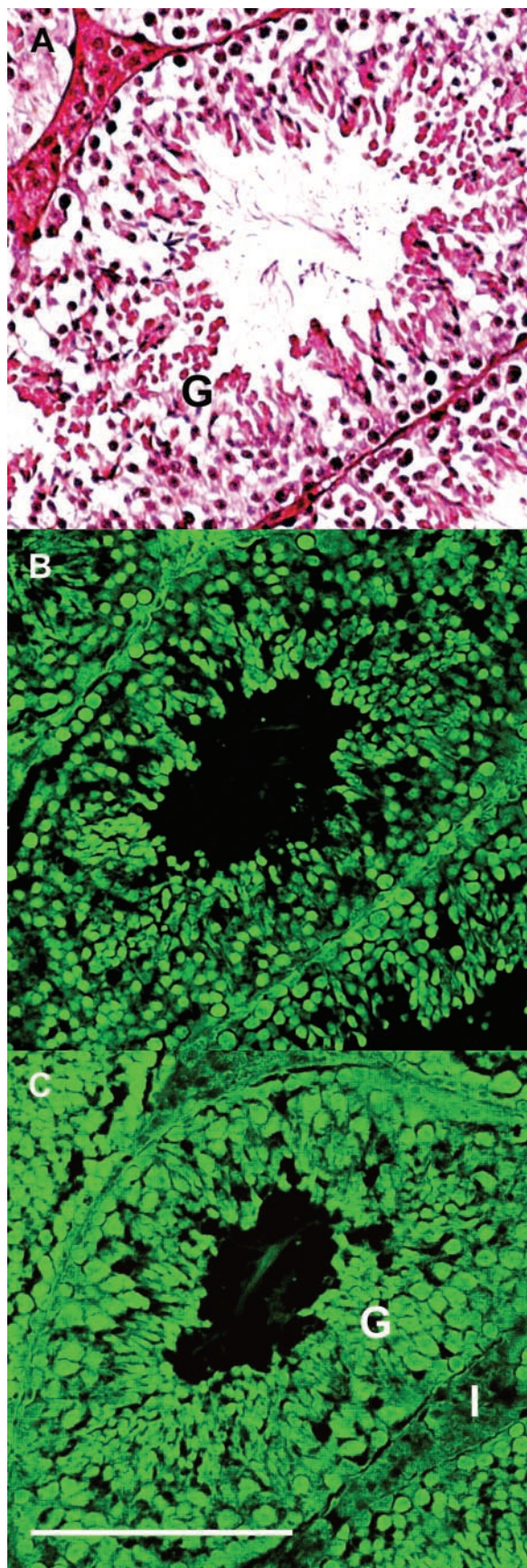
cells. Flux through a CCTβ2-dependent pathway for PtdCho production associated with membrane trafficking may support a turnover pathway stimulated by a growth factor(s) (29), thus leading to the failure to maintain differentiated ovaries in CCTβ2$^{-/-}$ mice. This latter idea is supported by recent work with the *Drosophila* system that implicates CCT in EGF receptor and Notch signaling (60), where disruption of one of two CCT genes leads to defective ovarian morphogenesis (24). Flies deficient in *CCT1* have reduced signal transduction through these two pathways that correlates with an increase in the sequestration of EGF receptors in an enlarged endocytic compartment. The genetic connection between *CCT1*, *Egfr*, and *Notch* (60) supports an emerging role for PtdCho metabolism in metazoan vesicular trafficking (6, 27). Future work with the CCTβ2$^{-/-}$ mice will investigate this hypothesis in more detail.

The real-time PCR data indicate that both CCTα and CCTβ2 transcripts increase during neurite outgrowth of PC12 cells. The inconsistency of this result with those recently reported (12) may be explained by the limited linear range, particularly at the high end of the scale, of the visual detection used in conventional RT-PCR methodology compared to that of the multilog linear range for amplicons in the real-time PCR assays used here. Our data (Fig. 5) and those of Araki and Wurtman (1) show that CCT expression and enzyme activity are not selectively regulated by NGF treatment of PC12 cells. Rather, both CCTα and CCTβ2 increase in a ratio of about 2:1, and these data agree with the expression measurements in the mouse brain. Also, the lack of a neural phenotype argues that CCTβ2 expression is not an essential component of NGF signaling as compared to the severe defect in neuronal cell survival in mice lacking the NGF receptor (16).

In general, CCTβ2 transcripts are found at levels 10-fold lower than those encoding CCTα, and therefore CCTβ2 is likely to contribute only a small percentage of the CDP-Cho required for a tissue to sustain bulk PtdCho synthesis. If the steady-state mRNA abundance reflects the relative amount of CCT isoforms in cells, then CCTβ2 usually contributes 10% or less to the total CCT activity in most tissues. The exception is brain, where CCTβ transcripts are approximately in equal abundance with CCTα, and CCTβ3 transcripts constitute a small portion of the CCT pool (Fig. 1). This selective expression pattern still may suggest a specific role for CCTβ2 in brain physiology, and future work will investigate the development of primary neurons in a more detailed manner. Our data with CCTβ2-deficient mice, together with the results in mice with a macrophage-specific CCTα deletion (66), suggest that CCT

FIG. 11. Fluorescent immunocytochemistry of CCT expression in testis. Wild-type 129/Sv × C57BL/6J testis (age, 4 months) was fixed and stained with hematoxylin and eosin (A), rabbit anti-mouse CCTα antibody (B), or rabbit anti-human CCTβ antibody (C), followed by goat anti-rabbit Alexa Fluor 488-coupled secondary IgG (H + L). Substitution of preimmune rabbit serum for the primary antibody did not yield a fluorescent image at the same exposure. Structures indicated are the following: G, seminiferous tubules and germinal cell layers; I, interstitial Leydig cells. CCTα is expressed in the seminiferous and germinal cell layers (B), and CCTβ is expressed in the same cell populations and at lower intensity in the interstitial Leydig cells (C). Scale bar, 0.1 mm.

expression is in excess in most wild-type primary cells and that selected cell types can increase CCT expression when the PtdCho synthetic capacity for normal growth and function is challenged.

ACKNOWLEDGMENTS

REFERENCES

1. **Araki, W., and R. J. Wurtman.** 1997. Control of membrane phosphatidylcholine biosynthesis by diacylglycerol levels in neuronal cells undergoing neurite outgrowth. Proc. Natl. Acad. Sci. USA **94:**11946–11950.
2. **Arnold, R. S., and R. B. Cornell.** 1996. Lipid regulation of CTP:phosphocholine cytidylyltransferase: electrostatic, hydrophobic, and synergistic interactions of anionic phospholipids and diacylglycerol. Biochemistry **35:**9917–9924.
3. **Arnold, R. S., A. A. DePaoli-Roach, and R. B. Cornell.** 1997. Binding of CTP:phosphocholine cytidylyltransferase to lipid vesicles: diacylglycerol and enzyme dephosphorylation increase the affinity for negatively charged membranes. Biochemistry **36:**6149–6156.
4. **Attard, G. S., R. H. Templer, W. S. Smith, A. N. Hunt, and S. Jackowski.** 2000. Modulation of CTP:phosphocholine cytidylyltransferase by membrane curvature elastic stress. Proc. Natl. Acad. Sci. USA **97:**9032–9036.
5. **Baburina, I., and S. Jackowski.** 1999. Cellular responses to excess phospholipid. J. Biol. Chem. **274:**9400–9408.
6. **Bankaitis, V. A., and A. J. Morris.** 2003. Lipids and the exocytotic machinery of eukaryotic cells. Curr. Opin. Cell Biol. **15:**389–395.
7. **Barbour, S. E., A. Kapur, and C. L. Deal.** 1999. Regulation of phosphatidylcholine homeostasis by calcium-independent phospholipase A_2. Biochim. Biophys. Acta **1439:**77–88.
8. **Bligh, E. G., and W. J. Dyer.** 1959. A rapid method of total lipid extraction and purification. Can. J. Biochem. Physiol. **37:**911–917.
9. **Bodensteiner, K. J., K. P. McNatty, C. M. Clay, C. L. Moeller, and H. R. Sawyer.** 2000. Expression of growth and differentiation factor-9 in the ovaries of fetal sheep homozygous or heterozygous for the inverdale prolificacy gene (FecX(I)). Biol. Reprod. **62:**1479–1485.
10. **Bradford, M. M.** 1976. A rapid and sensitive method for quantitation of microgram quantities of protein utilizing the principle of protein-dye binding. Anal. Biochem. **72:**248–254.
11. **Braw-Tal, R., K. P. McNatty, P. Smith, D. A. Heath, N. L. Hudson, D. J. Phillips, B. J. McLeod, and G. H. Davis.** 1993. Ovaries of ewes homozygous for the X-linked Inverdale gene (FecXI) are devoid of secondary and tertiary follicles but contain many abnormal structures. Biol. Reprod. **49:**895–907.
12. **Carter, J. M., K. A. Waite, R. B. Campenot, J. E. Vance, and D. E. Vance.** 2003. Enhanced expression and activation of CTP:phosphocholine cytidylyltransferase β2 during neurite outgrowth. J. Biol. Chem. **278:**44988–44994.
13. **Chabot, B., D. A. Stephenson, V. M. Chapman, P. Besmer, and A. Bernstein.** 1988. The proto-oncogene c-*kit* encoding a transmembrane tyrosine kinase receptor maps to the mouse *W* locus. Nature (London) **335:**88–89.
14. **Chiu, C.-H., and S. Jackowski.** 2001. Role of calcium-independent phospholipase (iPLA$_2$) in phosphatidylcholine metabolism. Biochem. Biophys. Res. Commun. **287:**600–606.
15. **Clement, J. M., and C. Kent.** 1999. CTP:phosphocholine cytidylyltransferase: insights into regulatory mechanisms and novel functions. Biochem. Biophys. Res. Commun. **257:**643–650.
16. **Conover, J. C., and G. D. Yancopoulos.** 1997. Neurotrophin regulation of the developing nervous system: analyses of knockout mice. Rev. Neurosci. **8:**13–27.
17. **Cornell, R. B., and I. C. Northwood.** 2000. Regulation of CTP:phosphocholine cytidylyltransferase by amphitropism and relocalization. Trends Biochem. Sci. **25:**441–447.
18. **Craig, L., J. E. Johnson, and R. B. Cornell.** 1994. Identification of the membrane-binding domain of rat liver CTP:phosphocholine cytidylyltransferase using chymotrypsin proteolysis. J. Biol. Chem. **269:**3311–3317.
19. **Davies, S. M., R. M. Epand, R. Kraayenhof, and R. B. Cornell.** 2001. Regulation of CTP:phosphocholine cytidylyltransferase activity by the physical properties of lipid membranes: an important role for stored curvature strain energy. Biochemistry **40:**10522–10531.
20. **Dunne, S. J., R. B. Cornell, J. E. Johnson, N. R. Glover, and A. S. Tracey.** 1996. Structure of the membrane binding domain of CTP:phosphocholine cytidylyltransferase. Biochemistry **35:**11975–11984.
21. **Galloway, S. M., K. P. McNatty, L. M. Cambridge, M. P. Laitinen, J. L. Juengel, T. S. Jokiranta, R. J. McLaren, K. Luiro, K. G. Dodds, G. W. Montgomery, A. E. Beattie, G. H. Davis, and O. Ritvos.** 2000. Mutations in an oocyte-derived growth factor gene (BMP15) cause increased ovulation rate and infertility in a dosage-sensitive manner. Nat. Genet. **25:**279–283.
22. **Greene, L. A.** 1978. Nerve growth factor prevents the death and stimulates the neuronal differentiation of clonal PC12 pheochromocytoma cells in serum-free medium. J. Cell Biol. **78:**747–755.
23. **Greene, L. A., and A. S. Tischler.** 1976. Establishment of a noradrenergic clonal line of rat adrenal pheochromocytoma cells which respond to nerve growth factor. Proc. Natl. Acad. Sci. USA **73:**2424–2428.
24. **Gupta, T., and T. Schüpbach.** 2003. Cct1, a phosphatidylcholine biosynthesis enzyme, is required for Drosophila oogenesis and ovarian morphogenesis. Development **130:**6075–6087.
25. **Hogan, B., R. Beddington, F. Costantini, and E. Lacy.** 1994. Manipulating the mouse embryo. Cold Spring Harbor Laboratory Press, Plainview, N.Y.
26. **Huang, E., A. Nocka, D. R. Beier, T. Y. Chu, J. Buck, H. W. Lahm, D. Wellner, P. Leder, and P. Besmer.** 1990. The hematopoietic growth factor KL is encoded by the Sl locus and is the ligand of the c-*kit* receptor. Cell **63:**225–233.
27. **Huijbregts, R. P., L. Topalof, and V. A. Bankaitis.** 2000. Lipid metabolism and regulation of membrane trafficking. Traffic **1:**195–202.
28. **Hunt, A. N., G. T. Clark, G. S. Attard, and A. D. Postle.** 2001. Highly saturated endonuclear phosphatidylcholine is synthesized in situ and colocated with CDP-choline pathway enzymes. J. Biol. Chem. **276:**8492–8499.
29. **Jackowski, S.** 1994. Coordination of membrane phospholipid synthesis with the cell cycle. J. Biol. Chem. **269:**3858–3867.
30. **Johnson, J. E., R. Aebersold, and R. B. Cornell.** 1997. An amphipathic α-helix is the principle membrane-embedded region of CTP:phosphocholine cytidylyltransferase. Identification of the 3-(trifluoromethyl)-3*m*[^{125}I](iodophenyl) diazirine photolabeled domain. Biochim. Biophys. Acta **1324:**273–284.
31. **Johnson, J. E., and R. B. Cornell.** 1994. Membrane-binding amphipathic α-helical peptide derived from CTP:phosphocholine cytidylyltransferase. Biochem. J. **33:**4327–4335.
32. **Karim, M., P. Jackson, and S. Jackowski.** 2003. Gene structure, expression and identification of a new CTP:phosphocholine cytidylyltransferase beta isoform. Biochim. Biophys. Acta **1633:**1–12.
33. **Kumar, T. R., Y. Wang, N. Lu, and M. M. Matzuk.** 1997. Follicle stimulating hormone is required for ovarian follicle maturation but not male fertility. Nat. Genet. **15:**201–204.
34. **Lagace, T. A., J. R. Miller, and N. D. Ridgway.** 2002. Caspase processing and nuclear export of CTP:phosphocholine cytidylyltransferase alpha during farnesol-induced apoptosis. Mol. Cell. Biol. **22:**4851–4862.
35. **Lykidis, A., I. Baburina, and S. Jackowski.** 1999. Distribution of CTP:phosphocholine cytidylyltransferase (CCT) isoforms. Identification of a new CCTβ splice variant. J. Biol. Chem. **274:**26992–27001.
36. **Lykidis, A., and S. Jackowski.** 2000. Regulation of mammalian cell membrane biosynthesis. Prog. Nucleic Acid Res. Mol. Biol. **65:**361–393.
37. **Lykidis, A., P. Jackson, and S. Jackowski.** 2001. Lipid activation of CTP:phosphocholine cytidylyltransferase α: characterization and identification of a second activation domain. Biochemistry **40:**494–503.
38. **Lykidis, A., K. G. Murti, and S. Jackowski.** 1998. Cloning and characterization of a second human CTP:phosphocholine cytidylyltransferase. J. Biol. Chem. **273:**14022–14029.
39. **Manova, K., E. J. Huang, M. Angeles, L. De, V., S. Sanchez, S. M. Pronovost, P. Besmer, and R. F. Bachvarova.** 1993. The expression pattern of the c-kit ligand in gonads of mice supports a role for the c-kit receptor in oocyte growth and in proliferation of spermatogonia. Dev. Biol. **157:**85–99.
40. **Matzuk, M. M.** 2000. Revelations of ovarian follicle biology from gene knockout mice. Mol. Cell Endocrinol. **163:**61–66.
41. **McLaren, A.** 1991. Development of the mammalian gonad: the fate of the supporting cell lineage. Bioessays **13:**151–156.
42. **McLaren, A.** 1995. Germ cells and germ cell sex. Philos. Trans. R. Soc. Lond. B. Biol. Sci. **350:**229–233.
43. **Nocka, K., S. Majumder, B. Chabot, P. Ray, M. Cervone, A. Bernstein, and P. Besmer.** 1989. Expression of c-*kit* gene products in known cellular targets of *W* mutations in normal and *W* mutant mice—evidence for an impaired c-*kit* kinase in mutant mice. Genes Dev. **3:**816–826.
44. **Noga, A. A., and D. E. Vance.** 2003. A gender-specific role for phosphatidylethanolamine N-methyltransferase-derived phosphatidylcholine in the regulation of plasma high density and very low density lipoproteins in mice. J. Biol. Chem. **278:**21851–21859.
45. **Northwood, I. C., A. H. Tong, B. Crawford, A. E. Drobnies, and R. B. Cornell.** 1999. Shuttling of CTP:phosphocholine cytidylyltransferase between the nucleus and endoplasmic reticulum accompanies the wave of phosphatidylcholine synthesis during the $G_0 \rightarrow G_1$ transition. J. Biol. Chem. **274:**26240–26248.
46. **Park, J. Y., Y. Q. Su, M. Ariga, E. Law, S.-L. C. Jin, and M. Conti.** 2004.

EGF-like growth factors as mediators of LH action in the ovulatory follicle. Science **303:**682–684.

47. **Park, Y. S., P. Gee, S. Sanker, E. J. Schurter, E. R. P. Zuiderweg, and C. Kent.** 1997. Identification of functional conserved residues of CTP:glycerol-3-phosphate cytidylyltransferase. J. Biol. Chem. **272:**15161–15166.

48. **Ridsdale, R., I. Tseu, J. Wang, and M. Post.** 2001. CTP:phosphocholine cytidylyltransferase alpha is a cytosolic protein in pulmonary epithelial cells and tissues. J. Biol. Chem. **276:**49148–49155.

49. **Smith, P., O. WS, K. A. Corrigan, T. Smith, T. Lundy, G. H. Davis, and K. P. McNatty.** 1997. Ovarian morphology and endocrine characteristics of female sheep fetuses that are heterozygous or homozygous for the inverdale pro-lificacy gene (fecX1). Biol. Reprod. **57:**1183–1192.

50. **Tischler, A. S., and L. A. Greene.** 1978. Morphologic and cytochemical properties of a clonal line of rat adrenal pheochromocytoma cells which respond to nerve growth factor. Lab. Investig. **39:**77–89.

51. **Veitch, D. P., and R. B. Cornell.** 1996. Substitution of serine for glycine-91 in the HXGH motif of CTP:phosphocholine cytidylyltransferase implicates this motif in CTP binding. Biochemistry **35:**10743–10750.

52. **Waite, K. A., N. R. Cabilio, and D. E. Vance.** 2002. Choline deficiency-induced liver damage is reversible in Pemt(−/−) mice. J. Nutr. **132:**68–71.

53. **Walkey, C. J., G. B. Kalmar, and R. B. Cornell.** 1994. Overexpression of rat liver CTP:phosphocholine cytidylyltransferase accelerates phosphatidylcholine synthesis and degradation. J. Biol. Chem. **269:**5742–5749.

54. **Walkey, C. J., L. Yu, L. B. Agellon, and D. E. Vance.** 1998. Biochemical and evolutionary significance of phospholipid methylation. J. Biol. Chem. **273:**27043–27046.

55. **Wang, Y., and C. Kent.** 1995. Effects of altered phosphorylation sites on the properties of CTP:phosphocholine cytidylyltransferase. J. Biol. Chem. **270:**17843–17849.

56. **Wang, Y., and C. Kent.** 1995. Identification of an inhibitory domain of CTP:phosphocholine cytidylyltransferase. J. Biol. Chem. **270:**18948–18952.

57. **Wang, Y., J. I. S. MacDonald, and C. Kent.** 1995. Identification of the nuclear localization signal of rat liver CTP:phosphocholine cytidylyltransferase. J. Biol. Chem. **270:**354–360.

58. **Wang, Y., T. D. Sweitzer, P. A. Weinhold, and C. Kent.** 1993. Nuclear

59. **Weber, C. H., Y. S. Park, S. Sanker, C. Kent, and M. L. Ludwig.** 1999. A prototypical cytidylyltransferase: CTP:glycerol-3-phosphate cytidylyltransferase from *Bacillus subtilis*. Structure Fold. Des. **7:**1113–1124.

60. **Weber, U., C. Eroglu, and M. Mlodzik.** 2003. Phospholipid membrane composition affects EGF receptor and notch signaling through effects on endocytosis during *Drosophila* development. Dev. Cell. **5:**559–570.

61. **Weiss, J., L. Axelrod, R. W. Whitcomb, P. E. Harris, W. F. Crowley, and J. L. Jameson.** 1992. Hypogonadism caused by a single amino acid substitution in the beta subunit of luteinizing hormone. N. Engl. J. Med. **326:**179–183.

62. **Wu, X., and M. M. Matzuk.** 2002. GDF-9 and BMP-15: oocyte organizers. Rev. Endocr. Metab. Disord. **3:**27–32.

63. **Xiong, Y., X.-L. Liu, Y. Wang, and Y.-C. Du.** 2000. Cloning of cytidine triphosphate:phosphocholine cytidylyltransferase mRNA upregulated by a neuropeptide arginine-vasopressin$_{(4-8)}$ in rat hippocampus. Neurosci. Lett. **283:**129–132.

64. **Yang, W., K. P. Boggs, and S. Jackowski.** 1995. The association of lipid activators with the amphipathic helical domain of CTP:phosphocholine cytidylyltransferase accelerates catalysis by increasing the affinity of the enzyme for CTP. J. Biol. Chem. **270:**23951–23957.

65. **Yang, W., and S. Jackowski.** 1995. Lipid activation of CTP:phosphocholine cytidylyltransferase is regulated by the phosphorylated carboxy terminal domain. J. Biol. Chem. **270:**16503–16506.

66. **Zhang, D., W. Tang, P. M. Yao, C. Yang, B. Xie, S. Jackowski, and I. Tabas.** 2000. Macrophages deficient in CTP:phosphocholine cytidylyltransferase-α are viable under normal culture conditions but are highly susceptible to free cholesterol-induced death. Molecular genetic evidence that the induction of phosphatidylcholine biosynthesis in free cholesterol-loaded macrophages is an adaptive response. J. Biol. Chem. **275:**35368–35376.

67. **Zsebo, K. M., D. A. Williams, E. N. Geissler, V. C. Broudy, F. H. Martin, H. L. Atkins, R. Y. Hsu, N. C. Birkett, K. H. Okino, D. C. Murdock, F. W. Jackobsen, K. E. Langley, K. A. Smith, T. Takeishi, B. M. Cattacnach, S. J. Galli, and S. V. Suggs.** 1990. Stem cell factor is encoded at the *Sl* locus of the mouse and is the ligand for the c-*kit* tyrosine kinase receptor. Cell **63:**213–224.